Earth and Planetary Science Letters 407 (2014) 82–95

Contents lists available at ScienceDirect

Earth and Planetary Science Letters

www.elsevier.com/locate/epsl

Cyclostratigraphy and orbital tuning of the terrestrial upper Santonian–Lower Danian in Songliao Basin, northeastern China

Huaichun Wu [a,b,*], Shihong Zhang [a], Linda A. Hinnov [c], Ganqing Jiang [d], Tianshui Yang [a], Haiyan Li [a], Xiaoqiao Wan [a], Chengshan Wang [a]

[a] *State Key Laboratory of Biogeology and Environmental Geology, China University of Geosciences (Beijing), Beijing 100083, China*
[b] *School of Ocean Sciences, China University of Geosciences (Beijing), Beijing 100083, China*
[c] *Department of Earth and Planetary Sciences, Johns Hopkins University, Baltimore, MD 21218, USA*
[d] *Department of Geoscience, University of Nevada, Las Vegas, NV 89154, USA*

ARTICLE INFO

Article history:
Received 5 June 2014
Received in revised form 15 September 2014
Accepted 18 September 2014
Available online 9 October 2014
Editor: J. Lynch-Stieglitz

Keywords:
Late Cretaceous
cyclostratigraphy
astronomical time scale (ATS)
SK-1n borehole
continental environment
Songliao Basin

ABSTRACT

The Songke-1 north (SK-1n) borehole recovered a continuous, 1541.66 m Late Santonian–Early Danian terrestrial succession in Songliao Basin (SB), northeastern China. It provides a unique record for improving our understanding of continental paleoclimate and ecological system in Cretaceous greenhouse world. Here we use thorium (Th) logging data as a paleoenvironmental and paleoclimatic proxy to conduct a detailed cyclostratigraphic study on the SK-1n core. Power spectra, evolutionary fast Fourier transformation and wavelet analysis all reveal significant decameter- to meter-scale sedimentary cycles in the Nenjiang (K_2n), Sifangtai (K_2s) and Mingshui (K_2m) formations. The ratios of cycle wavelengths in these stratigraphic units are ∼20:5:2:1, and are interpreted as Milankovitch cycles of 405 kyr and 100 kyr eccentricity, 38.4 kyr obliquity and 20 kyr precession cycles, respectively. An astronomical time scale (ATS) is established by tuning filtered 405 kyr eccentricity cycles to a target curve of the astronomical solution La2010d based on the magnetostratigraphic time framework of the SK-1n borehole. This ATS provides precise numerical ages for stratigraphic boundaries, biozones, geological and geophysical events, and serves as a basis for correlation of strata and events between marine and terrestrial systems. The Cretaceous/Paleogene (K/Pg), Campanian/Maastrichtian, Santonian/Campanian boundaries are estimated at core depths of 318 m, 752.8 m and 1751.1 m, respectively. A ∼3.8 myr-long hiatus between the Nenjiang (K_2n) and Sifangtai (K_2s) formations occurs from 76.1 to 79.9 million years ago. The ages and durations of magnetochrons C33r to C30n are precisely estimated and provide new constraints on the Late Cretaceous Geomagnetic Polarity Time Scale (GPTS) and South Atlantic sea-floor spreading rates.

© 2014 Elsevier B.V. All rights reserved.

1. Introduction

The Cretaceous represents one of the most remarkable periods in Earth history with a "greenhouse climate". However, our knowledge of Cretaceous terrestrial climatic change is sparse due in large part to a fragmentary continental stratigraphic record. The Songliao Basin (SB) in northeastern China is one of the largest and long-lived Cretaceous continental basins in the world. A program of the "Cretaceous Continental Scientific Drilling Program of China (CCSD)" recovered two overlapping drillcores (SK-1n (north core) and SK-1s (south core)) with a total length of 2485.89 m and a 96.46% recovery in central part of the SB, covering Late Cretaceous to Early Paleocene strata (Feng et al., 2013; Wang et al., 2013a). These cores provide a unique opportunity for studying the continental climate/environmental changes in the Cretaceous greenhouse world (e.g., Xi et al., 2012; Chamberlain et al., 2013; Huang et al., 2013; Li et al., 2013; Song et al., 2013; Wan et al., 2013).

Establishing a high-resolution chronostratigraphic framework for these drillcores is the essential first step for studying the terrestrial paleoclimate signals and their correlation with marine records. Due to the lack of common fossils, biostratigraphic correlation between terrestrial and marine deposits has been difficult (Scott et al., 2012; Wan et al., 2013). Consequently, intensive efforts have been focused on non-biostratigraphic methods such as magnetostratigraphy and radiometric isotopic geochronology. The available time framework for the SK-1 boreholes was established with geomagnetic polarity sequence from upper chron C34n to lower chron C29r, four SIMS U–Pb zircon ages, and biostratigraphic

* Corresponding author at: School of Ocean Sciences, China University of Geosciences (Beijing), Beijing 100083, China.
E-mail addresses: whcgeo@cugb.edu.cn (H. Wu), whccugb@hotmail.com (H. Wu).

http://dx.doi.org/10.1016/j.epsl.2014.09.038
0012-821X/© 2014 Elsevier B.V. All rights reserved.

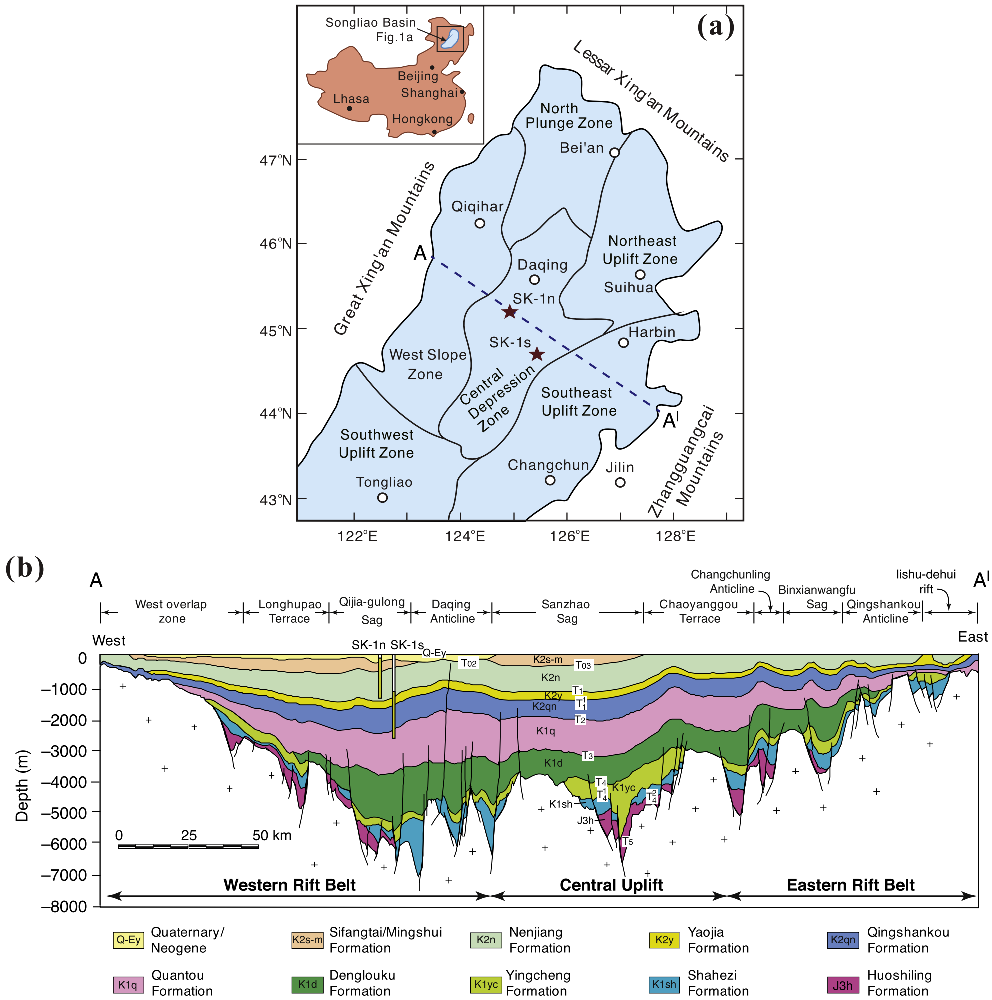

Fig. 1. (a) Schematic map showing the distribution of first-order tectonic units and location of the SK-1n and SK-1s boreholes in the Songliao Basin. (b) Structural cross section (A–A′) across the central part of the Songliao Basin based on regional seismic analyses (modified from Feng et al., 2010). The yellow bars in the SK-1n and SK-1s are cored intervals and the white bars are un-cored intervals. (For interpretation of the references to color in this figure legend, the reader is referred to the web version of this article.)

data (He et al., 2012; Deng et al., 2013; Wan et al., 2013). This time framework marks a significant progress but absolute age constraints for many critical boundaries and durations of geological/paleoclimate events are still lacking.

As a new non-biostratigraphic dating tool, cyclostratigraphy can provide a high-resolution astronomical time scale (ATS) by tuning the cyclic stratigraphic records to astronomical solutions (Hinnov and Ogg, 2007; Wu et al., 2012, 2013a). The construction of the ATS is well underway for the Cenozoic–Mesozoic eras (Hinnov and Hilgen, 2012; Hinnov, 2013), and recent progress in cyclostratigraphic analysis of marine sedimentary series provided an almost full coverage of the "floating" Cretaceous ATS in the geologic time scale (e.g., Locklair and Sageman, 2008; Mitchell et al., 2008; Huang et al., 2010; Husson et al., 2011; Batenburg et al., 2012; Meyers et al., 2012; Thibault et al., 2012; Sprovieri et al., 2013; Laurin et al., 2014). The identification of Milankovitch cycles from the Cretaceous terrestrial records in northeastern China allowed us to establish a high resolution ATS for Cenomanian, Turonian and Coniacian strata, which sheds light on the possibility of the high-resolution correlation between marine and continental sections (Wu et al., 2009, 2013b, 2013c).

In this paper, we report a cyclostratigraphy analysis of Late Santonian to Early Paleogene lacustrine and fluvial deposits of the SK-1n borehole in the SB using thorium (Th) logging data. The aims of this study are 1) to provide a high-resolution ATS for the SK-1n core that is tuned to 405-kyr long orbital eccentricity curve of the La2010d astronomical model (Laskar et al., 2011a), 2) to recalibrate the ages and durations of major geological, geophysical, biological and environmental events in the SB, and 3) to precisely estimate the ages and durations of the magnetochrons C33r to C30n and improve the Late Cretaceous Geomagnetic Polarity Time Scale (GPTS).

2. Geological setting and SK-1n borehole

2.1. Geological setting

The SB covers roughly 260,000 km^2 in Heilongjiang, Jilin and Liaoning provinces in Northeastern China. Geographically it is approximately rhombic in shape, and is bordered by great Xing'an Mountains to the west, the Lesser Xing'an Mountains to the north and the Zhangguangcai Mountains to the east (Fig. 1a). Tectonically, the SB has been interpreted as formed by extension associated with westward subduction of the paleo-Pacific plate underneath the Asian continental margin and/or upwelling of a mantle plume (Okada, 2000). The basin underwent four major tectonic events: mantle upwelling, rifting, post-rift thermal subsidence and structural inversion (Wang et al., 2007; Feng et al., 2010).

The basement of the SB consists of Precambrian to Paleozoic metamorphic and igneous rocks and Paleozoic to Mesozoic granites (Wang et al., 2006; Pei et al., 2007). Unconformably overlying the basement, up to 7000-m-thick Mesozoic and Cenozoic terrestrial strata are unevenly distributed across the basin (Gao et al., 1994) (Fig. 1b). The Late Jurassic, Cretaceous and Cenozoic strata can be divided into thirteen lithologic formations, including the Huoshiling (J_3h), Shahezi (K_1s), Yingcheng (K_1y), Denglouku (K_1d), Quantou (K_2q), Qingshankou (K_2qn), Yaojia (K_2y), Nenjiang (K_2n), Sifangtai (K_2s), Mingshui (K_2m), Yi'an (E_2y), Da'an (N_1d) and Taikang (N_2t) formations (Ren et al., 2002; Wang et al., 2007; Feng et al., 2010) (Fig. 1b). Recently, the Mesozoic–Cenozoic boundary was identified in the upper Mingshui Formation (Li et al., 2011; Wan et al., 2013), which is unconformably overlain by Cenozoic stratigraphic units including Yi'an (E_2y), Da'an (N_1d) or Taikang (N_2t) formations or Quaternary sediments (Fig. 1b). The source of terrigenous clastic sediments varied through time but was mainly from the northwest (Wang et al., 2013b).

The paleoclimate during the Cretaceous in the SB was temperate and humid with relatively abundant rainfall according to climatologically sensitive deposits, oxygen isotope studies, and paleontology (Gao et al., 2013; Wang et al., 2013a). Long term paleoclimate changes, including four cooling, three warming and three semiarid events, were identified in the SB (Wang et al., 2013a). Large-scale pressure systems and prevailing wind directions revealed by CO_2 simulations show a remarkable monsoonal seasonal climate variation over East Asia at 66 Ma (Chen et al., 2013). Cyclostratigraphy study suggests that astronomical forcing had played an important role in climate change affecting SB (Wu et al., 2009, 2013c).

2.2. The SK-1n borehole

The SK-1n borehole was drilled in the south–central part of the SB in 2007 (Fig. 1a). The borehole was continuously cored with a 94.56% recovery and the total length of drillcores is 1541.66 m (Feng et al., 2013; Wang et al., 2013a). It is 77.35 km distant from the SK-1s borehole and can be correlated with SK-1s via the basin-wide oil shale in the lower Member 2 of the Nenjiang Formation (K_2n^2) (Fig. 1a). The strata in SK-1n include the Neogene Taikang Formation (N_2t), the Lower Paleogene and Upper Cretaceous Mingshui (K_2m) Formation, and Upper Cretaceous Sifangtai (K_2s) and Nenjiang (K_2n) formations in descending order (Feng et al., 2013; Wang et al., 2013a; Wan et al., 2013). A detailed core description of the lithology at the centimeter scale and related depositional features was conducted on the SK-1n core (Cheng et al., 2011; Gao et al., 2011; Wang et al., 2011a, 2011b).

The Mingshui Formation (K_2m) (210.7–807.12 m) is divided into two members. Member 1 (K_2m^1) is composed of interbedded purple–red with greyish green and grey mudstone, sandy mudstone and muddy siltstone, and Member 2 (K_2m^2) mainly consists of greenish grey, purple–red and greyish black mudstone, greyish green gravel-bearing mudstone, greyish green muddy siltstone and greyish green sandstone with conglomerate intercalations (Cheng et al., 2011; Wan et al., 2013) (Fig. 2). The depositional environments were meandering river and shallow lake (Cheng et al., 2011) (Fig. 2). The Mingshui Formation (K_2m) is unconformably overlain by the Neogene Taikang Formation (N_2t).

The Sifangtai Formation (K_2s) (807.12–1021.6 m) consists of purple–red, greyish green, black to grey mudstone, sandy mudstone, argillaceous siltstone and sandstone, which were deposited in meandering river and shallow lake environments (Wang et al., 2011a; Wan et al., 2013) (Fig. 3). It lies unconformably over the Nenjiang Formation (K_2n). Both Sifangtai (K_2s) and Mingshui (K_2m) formations were deposited during the waning phase of the basin's life (Feng et al., 2010).

The Nenjiang Formation (K_2n) (1021.6–1796.75 m) can be divided into five members (Fig. 4). Members 1 and 2 (K_2n^{1+2}) are dominated by deep-water lacustrine gray to black mudstone, marl, silty mudstone with a black to brown oil-shale bed at the base of Member 2. During deposition of Member 1 (K_2n^1), the lake expanded rapidly and reached its maximum, covering almost the entire basin. Members 3–5 are mainly composed of black mudstone, greyish black sandy mudstone, and grey siltstone and sandstone that were deposited in shallow lake, delta and meandering river environments (Wang et al., 2011b; Wan et al., 2013).

2.3. Sedimentary cycles

Nested orders of sedimentary cycles are well developed in the SK-1n borehole according to core lithology descriptions (Cheng et al., 2011; Gao et al., 2011; Wang et al., 2011a, 2011b), and a total of 3.5 third-order, 46 fourth-order, 323 fifth-order and 892 meter-scale sedimentary cycles were identified in K_2n^{2-5}, K_2s and K_2m (Wang et al., 2013b). The meter-scale sedimentary cycles are observed in variations of rock color, lithology and sedimentary facies, with thicknesses ranging from 0.4 m to 3.5 m. For example, the sedimentary facies of the upper part (845 m–920 m) of K_2s are predominantly meandering river and lacustrine that can be further divided into seven microfacies including crevasse splay, crevasse splay channel, floodplain, floodplain lake, undisturbed lake, natural levee and nearshore bar (Fig. 5; Wang et al., 2011a). The meter-scale sedimentary cycles are generally composed of couplets of nearshore bar sandstone and mudstone, floodplain muddy siltstone and floodplain lake mudstone, and 59 meter-scale sedimentary cycles with thicknesses ranging from 0.6–2.5 m were identified in this interval (Fig. 5; Wang et al., 2011a).

2.4. Magnetostratigraphic time constraints

Recently, Deng et al. (2013) identified eleven magnetozones with five reversed, five normal and one mixed polarities in the SK-1n cores (Figs. 2–4). The geomagnetic reversal in lower K_2n^2 was also identified at the same stratigraphic level of SK-1s, which was interpreted as the C34n/C33r boundary according to a SIMS U–Pb zircon age of 83.7 ± 0.8 Ma at the depth ∼31 m below it (He et al., 2012). Thus these magnetozones were correlated to chrons C29r (317.0–342.1 m), C30n–C31n (342.1–530.78 m), C31r (530.78–700.88 m), C32n (700.88–852.6 m), C32r.1r (852.6–887.8 m), C32r.1n (887.8–895.8 m), C32r.2r (895.8–910.2 m), C33n (910.2–1020.4 m) and C33r (1020.4–1739.3 m), respectively (Deng et al., 2013, Figs. 2–4). This magnetostratigraphic time framework provides a series of anchor and testing age points for constructing the ATS in this study.

3. Data and methods

3.1. Thorium (Th) logging data

GR (gamma-ray) and SGR (spectral gamma-ray) logging data, which relate to the amount of radioactive atomic nuclei of potassium (K), uranium (U) and thorium (Th) in the rock, have been widely used in paleoclimatic and paleoenvironmental research (e.g., Ten Veen and Postma, 1996; Schnyder et al., 2006; Laurin et al., 2014). Th is considered partially insoluble and concentrated during weathering, while U and K are more soluble than Th and thus prone to mobilization or concentration (Schnyder et al., 2006). In SK-1n GR and U logging data show abnormally high values in a number of beds of in K_2n^5, K_2s and K_2m^2 (Wang et al., 2013b), while Th data show relatively stable variations, closely tracking lithological changes, with high Th in the mudstones and low Th in the sandstones (Figs. 2–5). In this study, we use the Th logging data as a paleoclimatic and paleoenvironmental proxy for cyclostratigraphy analysis (Supplementary Table S1), as done previously on the Yaojia Formation (K_2y) of the SK-1s core (Wu et al., 2013c).

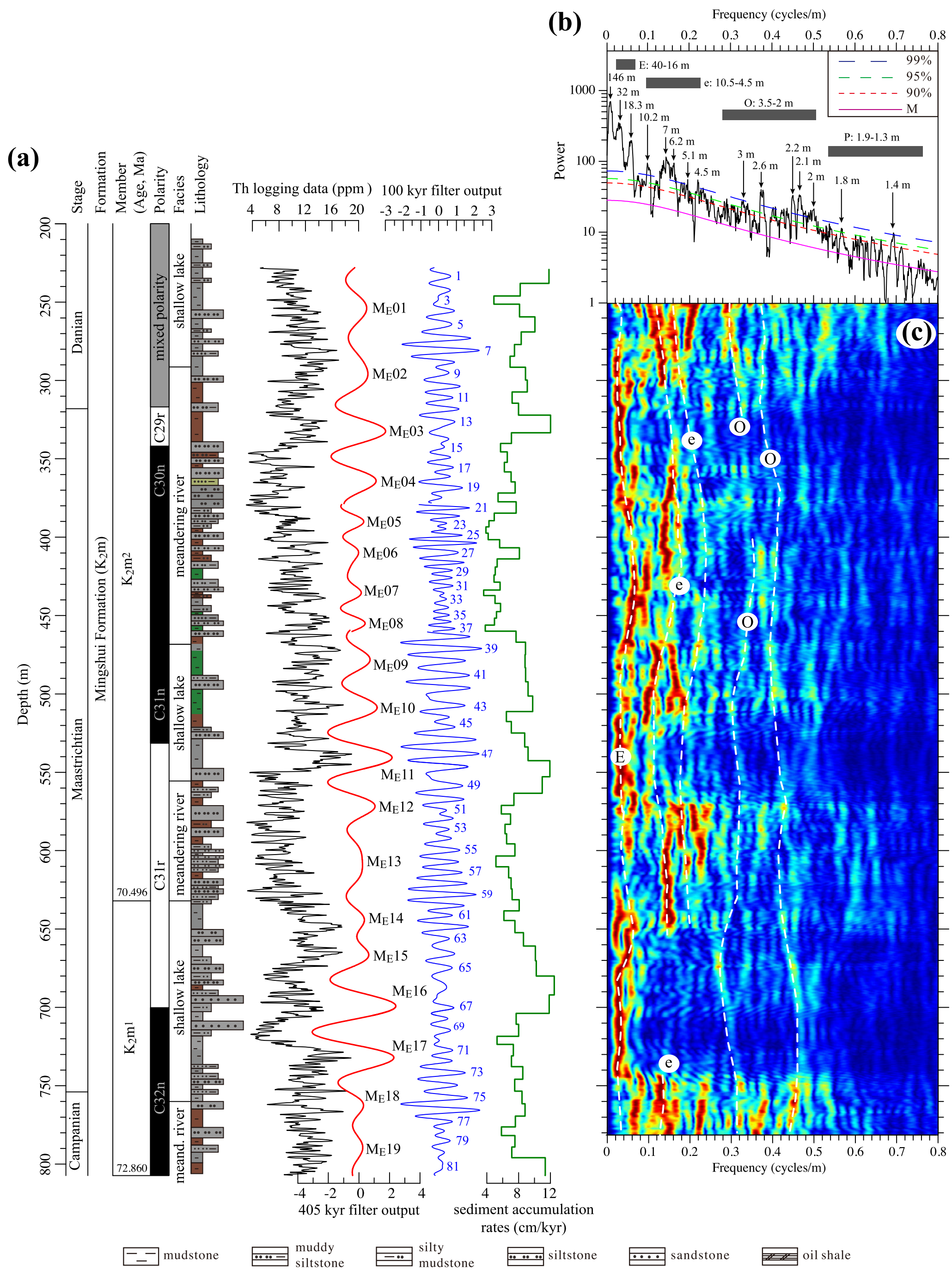

Fig. 2. (a) Magnetostratigraphy, sedimentary facies and lithology of the Mingshui Formation (K_2m) of SK-1n, with the Th logging data, interpreted 100-kyr and 405-kyr sedimentary cycles, and the calculated sediment accumulation rates. The interpreted 405-kyr (red) and 100-kyr (blue) cycles were extracted with Gaussian filters with passbands of 0.03 ± 0.01 cycles/m and 0.12 ± 0.04 cycles/m, respectively. For the data of the depth 379–460 m, we used passbands of 0.05 ± 0.009 cycles/m and 0.1 ± 0.005 cycles/m. Magnetostratigraphy results are from Deng et al. (2013), and paleoenvironmental data are from Cheng et al. (2011). (b) 2π MTM power spectrum of the untuned Th series of Mingshui Formation (K_2m). The purple, red, green and blue (dashed) curves represent the median smoothed, linear fitted red noise spectrum, and 90%, 95% and 99% confidence levels. (c) FFT spectrogram of the untuned Th series of K_2m. The sliding window is 40 m and the step rate is 0.5 m. The red and blue colors represent high and low power, normalized to 1. The dashed black lines labeled with E, e, O and P represent the 405-kyr eccentricity, 100-kyr eccentricity, obliquity and precession cycles, respectively. (For interpretation of the references to color in this figure legend, the reader is referred to the web version of this article.)

3.2. Time series methods

The Th logging series is detrended by subtracting a 35% weighted average in software Kaleidagraph™ (Cleveland, 1979). Power spectral analysis on the Th logging data was performed with the multitaper method (MTM) using the SSA-MTM toolkit (Ghil et al., 2002), with robust red noise modeling reported at the 90%, 95% and 99% confidence levels for interpretation of spectral peak significance (Mann and Lees, 1996). Evolutionary fast Fourier transform (FFT) spectrograms (Kodama and Hinnov, 2014) and wavelet analysis (Torrence and Compo, 1998) were also conducted on the Th series to identify the changes in cycle frequencies due to variable sedimentation rate. The cycle length ratio method was applied to investigate links between detected sedimentary cycle patterns and astronomical forcing (Mayer and Appel, 1999; Weedon, 2003). Gaussian bandpass filters were designed to extract

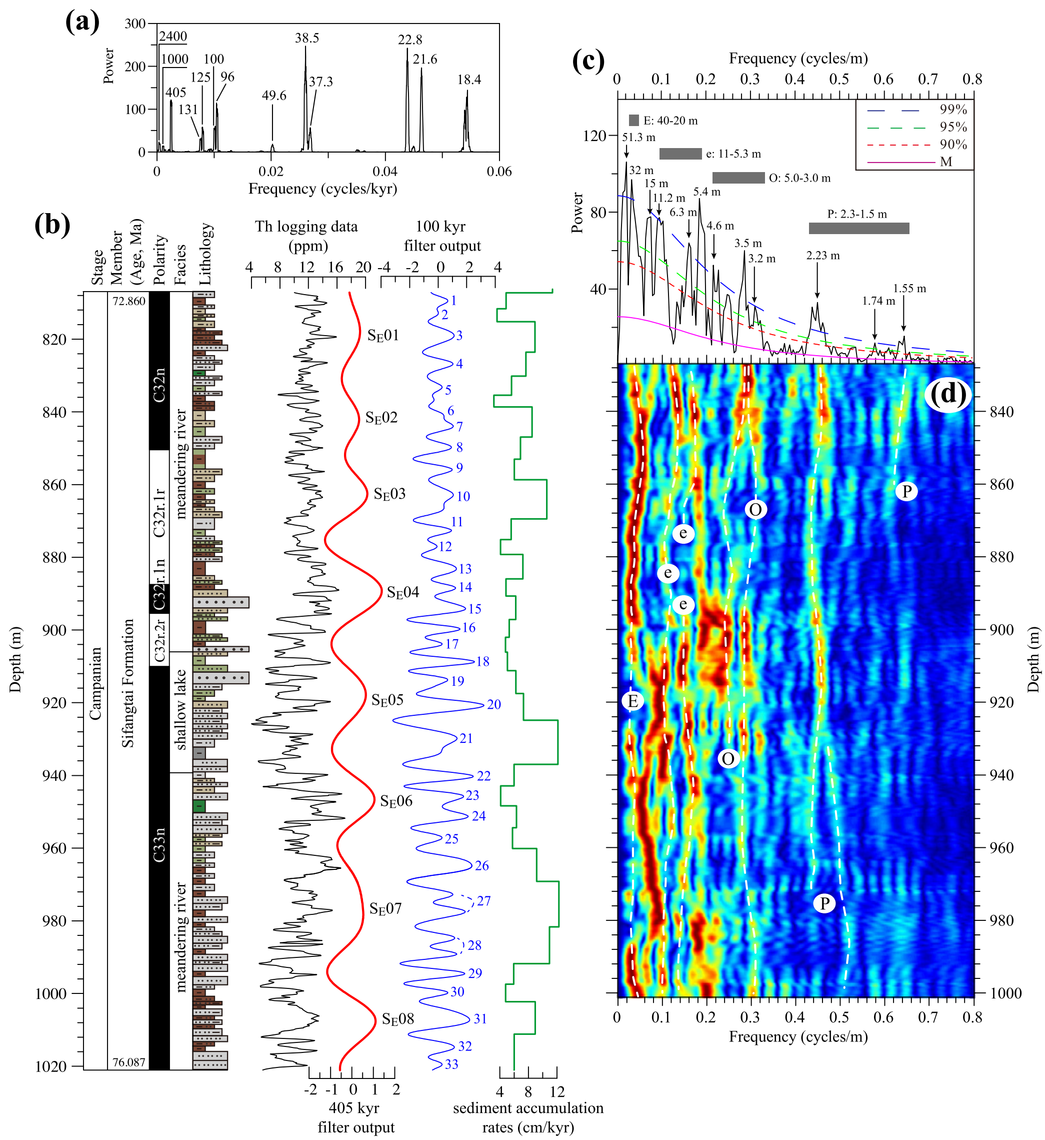

Fig. 3. (a) 2π MTM power spectrum of the ETP signal of the La2010d solution (Laskar et al., 2011a). (b) Magnetostratigraphy, sedimentary facies and lithology of the Sifangtai Formation (K_2s) of SK-1n, with the Th logging data, interpreted 405-kyr and 100-kyr sedimentary cycles, and the calculated sediment accumulation rates. The interpreted 405-kyr (red) and 100-kyr (blue) cycles were extracted with Gauss filters with passbands of 0.035 ± 0.015 cycles/m and 0.14 ± 0.1 cycles/m, respectively. Magnetostratigraphy results are from Deng et al. (2013), and paleoenvironmental data are from Wang et al. (2011a). (c) 2π MTM power spectrum and (d) FFT spectrogram of the untuned Th series of Sifangtai Formation (K_2s) with a 40 m sliding window and 0.5 m step. See legends and notes in Fig. 2. (For interpretation of the references to color in this figure legend, the reader is referred to the web version of this article.)

interpreted 405 kyr and 100 kyr eccentricity cycles. The filtering and tuning procedures were conducted in Analyseries 2.0.4.2 (Paillard et al., 1996).

3.3. Astronomical target curve

Both La2004 and La2010 astronomical solutions provide fundamental tools for refining the Cenozoic time scale (Laskar et al., 2004, 2011a). However, the full bands of the orbital parameters of the La2004 and La2010 solutions are considered to be valid only as far back as ∼42 Ma and ∼50 Ma, respectively. Before this time, solution accuracy decreases rapidly due to chaotic behavior of the Solar System and an inability of the solutions to predict this behavior. Only the 405-kyr eccentricity term remains stable and accurate, and can be used as a metronome for establishing a reliable Mesozoic ATS (Laskar et al., 2004).

The La2010 solution provides four eccentricity solutions including La2010a, b, c and d (Laskar et al., 2011a); La2010d is thought to represent the most reliable and valid solution over ∼54 Ma (Laskar et al., 2011b; Westerhold et al., 2012). Recently, the agreement of the U–Pb age-calibrated Late Permian 405 kyr cycles to La2010d indicate 405 kyr eccentricity cycles of the La2010d extend accurately back to 260 Ma (Wu et al., 2013a). Therefore, the 405-kyr eccentricity cycle of the La2010d is used as the tuning target curve in this study, which is isolated from the solution with a Gaussian passband of 0.002469 ± 0.0005 cycles/kyr.

4. Results

4.1. Cyclostratigraphic analysis

MTM power spectral analysis of the untuned Th series of the K_2m reveals significant sedimentary cycles at wavelengths of 32 m, 18.3 m, 10.2 m, 7 m, 6.2 m, 5.1 m, 3 m, 2.6 m, ∼2.1 m, 1.8 m and 1.4 m (Fig. 2b). The evolutionary FFT spectrogram additionally suggests variable sediment accumulation rates (SAR) (Fig. 2c). The ratio of the wavelengths of the 40–16 m, 10.5–4.5 m, 3.5–2 m and 1.9–1.3 m is approximately 20:5:2:1, which is consistent with the

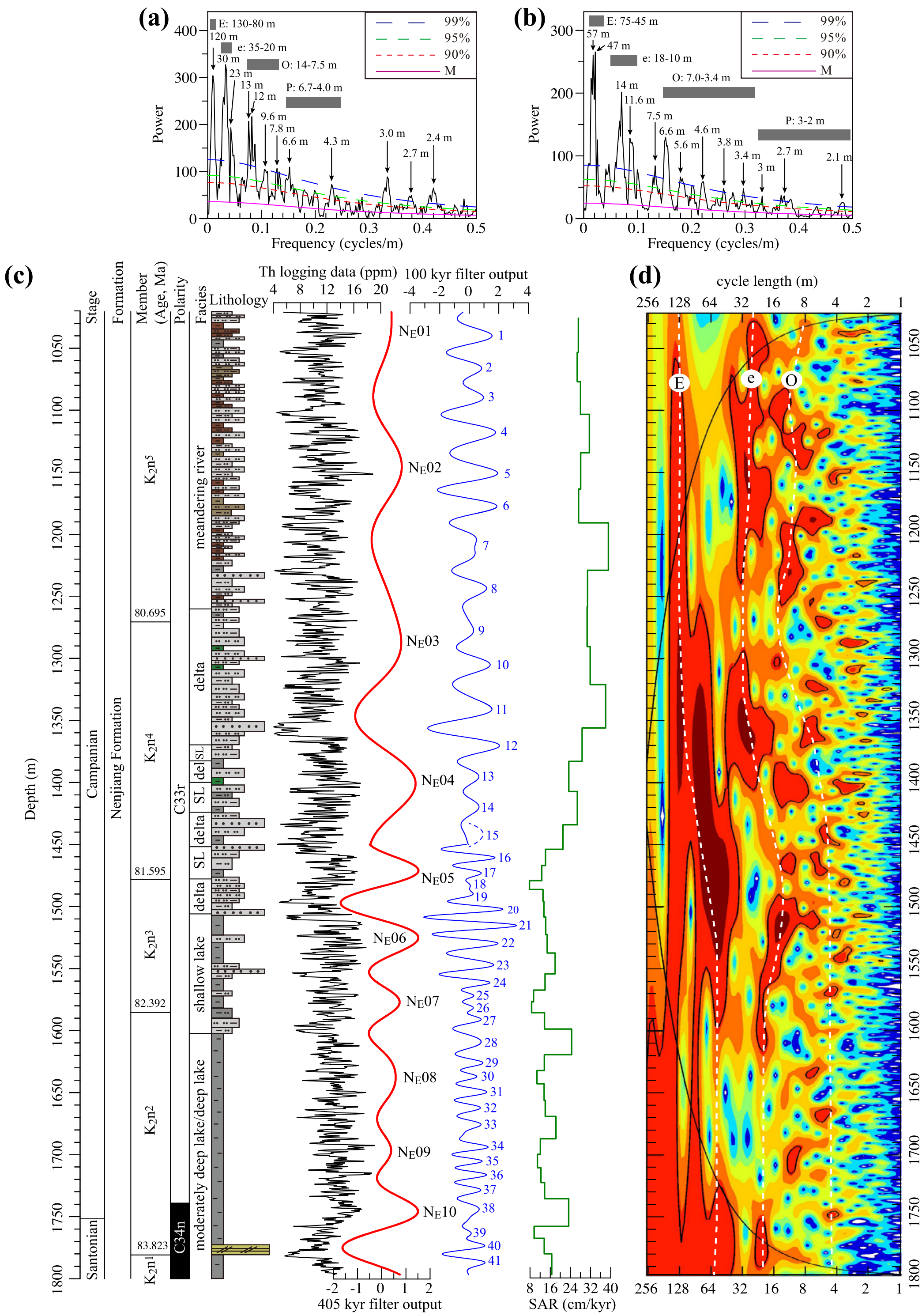

Fig. 4. Cyclostratigraphy of the Nenjiang Formation (K_2n) of the SK-1n borehole. 2π MTM power spectra of the untuned Th series for the depth interval of 1121.6–1450 m (a) and 1450–1790 m (b). (c) Magnetostratigraphy, sedimentary facies and lithological column of the K_2n of the SK-1n, with the Th logging data, interpreted 100-kyr and 405-kyr sedimentary cycles, and the calculated sediment accumulation rates. The interpreted 405-kyr (red) and 100-kyr (blue) cycles were extracted with Gauss filters with passbands of 0.008 ± 0.004 cycles/m and 0.033 ± 0.016 cycles/m (1121.6–1450 m), and 0.017 ± 0.008 cycles/m and 0.07 ± 0.03 cycles/m (1450–1790 m), respectively. Magnetostratigraphy is from Deng et al. (2013), and paleoenvironmental data are from Gao et al. (2011) and Wang et al. (2011b). (d) Morlet wavelet scalogram of the untuned Th series of K_2n. The shaded contours in wavelet scalograms are normalized linear variance, with blue representing low variance and red representing high variance. Regions below curves on both ends of the scalogram indicate the cone of influence where edge effects become significant. See legends and notes in Fig. 2. (For interpretation of the references to color in this figure legend, the reader is referred to the web version of this article.)

ratio of the Late Cretaceous orbital cycles (Fig. 3a). Thus we tentatively interpret the cycle bands to correspond to 405 kyr long eccentricity, 100 kyr short eccentricity, obliquity and precession cycles, respectively (Fig. 2).

The power spectrum and FFT spectrogram of the untuned Th series of K_2s reveal cycles with wavelengths of 51.3 m, 32 m, 15 m, 11.2 m, 6.3 m, 5.4 m, 4.6 m, 3.5 m, 3.2 m, 2.23 m, 1.74 m and 1.55 m (Fig. 3c, d). The ratio of these cycle wavelengths, i.e.,

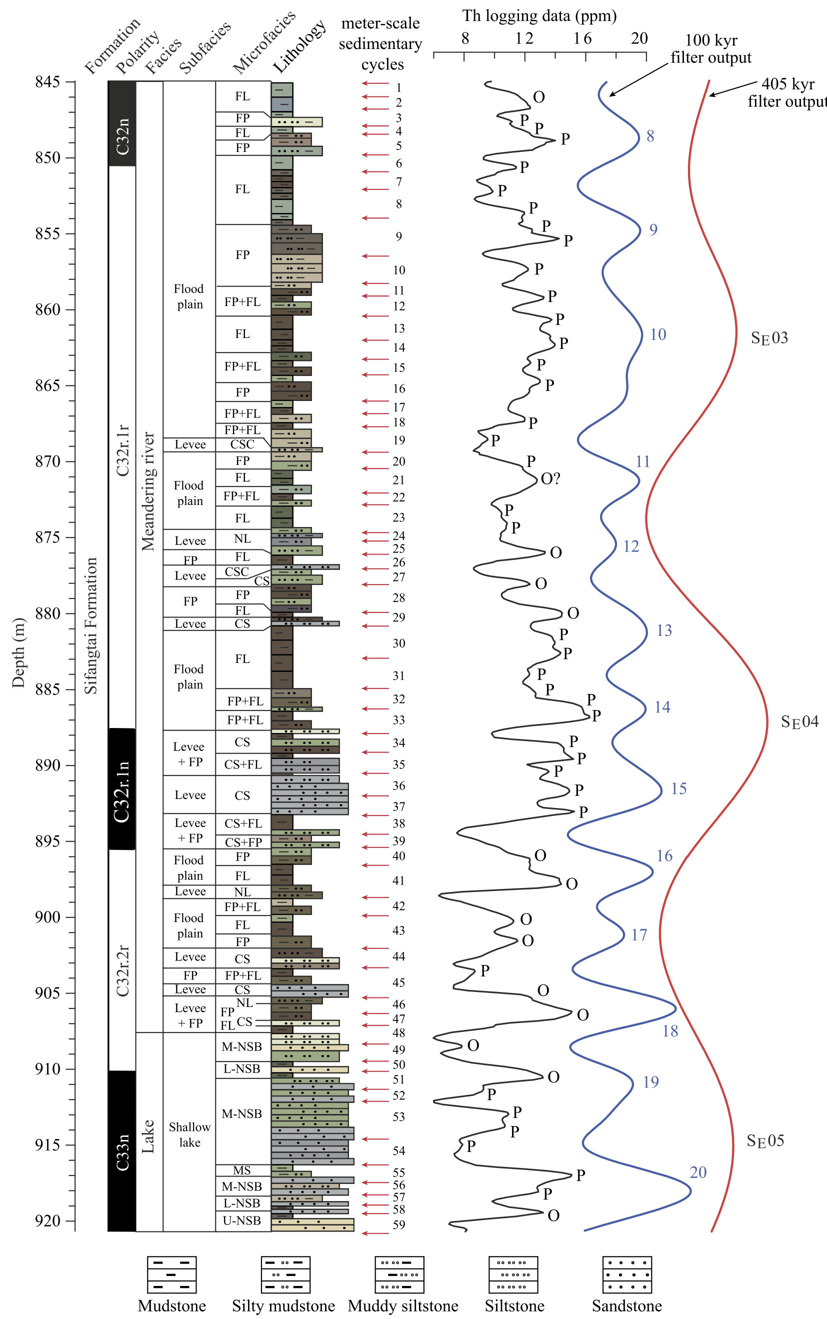

CS: crevasse splay; CSC: crevasse splay channel; FP: floodplain; FL: floodplain lake; MS: undisturbed water; NL: natural levee; U-NSB: upper nearshore bar; M-NSB: medium nearshore bar; L-NSB: lower nearshore bar

Fig. 5. Magnetostratigraphy, sedimentary facies, subfacies, microfacies, lithology and cyclostratigraphy of the upper Sifangtai Formation (K_2s) (845–921 m) of SK-1n. The interpreted 100-kyr (blue) and 405-kyr (red) cycles of the Th logging data were extracted with Gaussian filters with passbands of 0.14 ± 0.1 cycles/m and 0.035 ± 0.015 cycles/m, respectively. Magnetostratigraphy results are from Deng et al. (2013), and paleoenvironmental data and meter-scale sedimentary cycles are modified from Wang et al. (2011a). "P" and "O" represent precession and obliquity cycles. Cycle numbers are consistent with Fig. 3. (For interpretation of the references to color in this figure legend, the reader is referred to the web version of this article.)

40–20 m, 11–5.3 m, 5.0–3.0 m and 2.3–1.5 m might indicate they represent long, short eccentricity, obliquity and precession cycles, respectively (Fig. 3).

The wavelet spectrum of the untuned Th series of the K_2n shows an abrupt shift of the periods at the depth of ~1450 m, which may record a significant change in SAR (Fig. 4d). The power spectrum of the upper part of the K_2n reveals significant peaks with wavelengths of 120 m, 30 m, 23 m, 13 m, 12 m, 9.6 m, 7.8 m, 6.6 m, 4.3 m, 3.0 m, 2.7 m and 2.4 m. According to the cycle length ratio method and the magnetostratigraphic age framework (see Section 4.2), the sedimentary cycles of the 120 m, 20–35 m, 14–7.5 m and 6.7–4.0 m may be the long and short eccentricity, obliquity and precession cycles (Fig. 4a).

The power spectrum of the lower part of K_2n reveals significant peaks with wavelengths of 57 m, 47 m, 14 m, 11.6 m, 6.6 m, 5.6 m, 4.6 m, 3.8 m, 3.4 m, 2.7 m and 2.1 m. These are interpreted as long eccentricity (75–45 m), 100 kyr short eccentricity (18–10 m), obliquity (7.0–3.4 m), and precession cycles (2–3 m) (Fig. 4b).

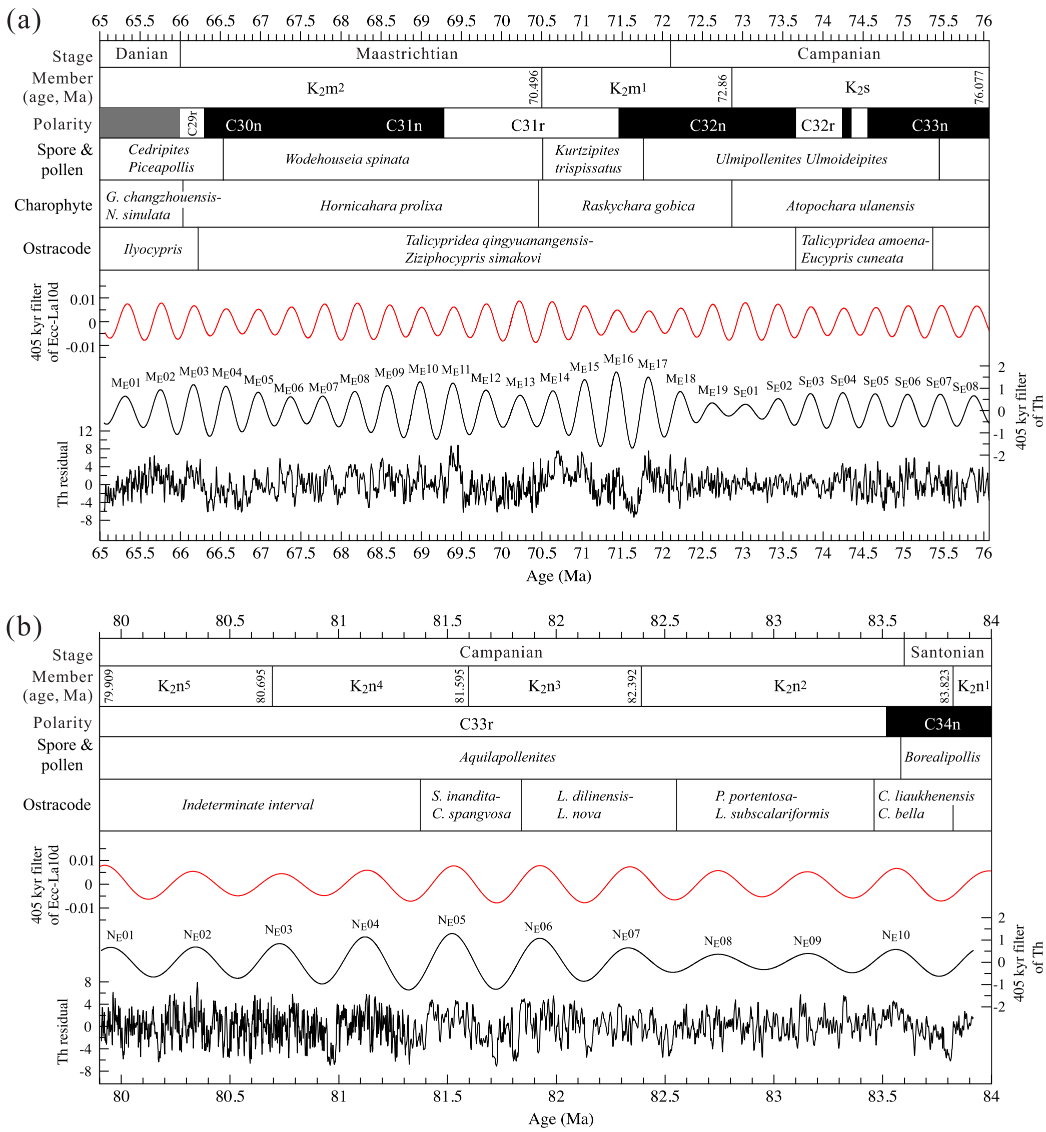

Fig. 6. Astrochronology age framework for the Mingshui (K_2m) and Sifangtai (K_2s) formations (a) and Nenjiang (K_2n) formations (b). Also shown from top are stages with boundary ages from GTS2012 (Gradstein et al., 2012), member boundary ages, magnetic polarity chrons with boundary ATS ages (Deng et al., 2013), microfossil zonations (Wan et al., 2013; Qu et al., 2014), extracted 405 kyr eccentricity cycles from La2010d (Laskar et al., 2011a) and 405 kyr-tuned Th logging data.

4.2. Initial age control and astronomical tuning of the SK-1n borehole

Because there is a major unconformity between the K_2s and K_2n, we separately tuned K_2m–K_2s and K_2n to the astronomical target curves. We used the age of the C30n/C29r reversal boundary as the initial age control for the K_2m and K_2s, and the C34n/C33r reversal boundary for K_2n. The C30n/C29r boundary is very close to a minimum 405-kyr eccentricity as observed in marine strata by Husson et al. (2011), Westerhold et al. (2008) and Batenburg et al. (2012). However, these authors provided two options for the ages of C30n/C29r and the K/Pg boundary with one 405 kyr eccentricity cycle difference. Recently, Gradstein et al. (2012) and Ogg (2012) adopted an age of 66.0 Ma for the K/Pg boundary and 66.3 Ma for the C30n/C29r boundary. In this study, 66.3 Ma (C30n/C29r boundary) and 83.6 Ma (C34n/C33r) of GTS2012 (Gradstein et al., 2012) were used as initial anchor points for the K_2m–K_2s and K_2n, respectively.

Gaussian bandpass filters were designed to extract the interpreted 405 kyr and 100 kyr eccentricity cycles in the SK-1n borehole. The K_2m, K_2s and K_2n record 19 (M_E01–19), 8 (S_E01–08) and 10 (N_E01–10) long (405 kyr) eccentricity cycles, and 81, 33 and 41 short (100 kyr) eccentricity cycles, respectively (Figs. 2–4).

We tuned the maxima of the filtered 405 kyr sedimentary cycles of the Th series to the maxima of the target 405 kyr eccentricity curve filtered from La2010d. The tuning was done by using the maximum of the first 405 kyr eccentricity cycle (M_E03) above C30n/C29r boundary, and M_E10 below the C34n/C33r boundary as the starting points for K_2m–K_2s and K_2n, respectively (Figs. 2–6).

There are three factors that determine the phase relationship between sedimentary cycles and astronomical target curves:

(1) It is well-known that amplitude of precession index is modulated by the orbital eccentricity (Laskar et al., 2004). In this study, the meter-scale sedimentary cycles and interpreted precession cycles in the Th series show very distinct variations during higher 405 kyr and 100 kyr filtered output, and also show that five or six interpreted precession cycles are bundled into one 100 kyr eccentricity cycle, and four 100 kyr eccentricity cycles are bundled into one 405 kyr eccentricity cycle (Fig. 5).

(2) The Th series generally shows that higher values correspond to higher mud content (Figs. 2–5). Wetter and warmer climate conditions could enhance chemical weathering and clay mineral

Table 1
ATS ages and durations for the ostracode, spore and pollen, and charophyte biozonations in the SK-1n borehole (Wan et al., 2013; Qu et al., 2014).

Ostracode	Depth (m)	Lower age, Ma (Durations, myr)	Spore & pollen	Depth (m)	Lower age, Ma (Durations, myr)	Charophyte	Depth (m)	Lower age, Ma (Durations, myr)
Ilyocypris	220–335.09	66.208	*Cedripites Piceapollis*	360.6	66.529	*Grovesichara changzhouensis–Neocahra sinulata*	299.7–328.8	66.13 (0.32)
Talicypridea qingyuanangensis Ziziphocypris simakovi	335.1–854	73.686 (7.478)	*Wodehouseia spinata*	360.6–635.4	70.51 (3.981)	*Hornicahara prolixa*	328.8–632.3	70.469 (4.339)
Talicypridea amoena–Eucypris cuneata	854–970	75.378 (1.692)	*Kurtzipites trispissatus*	635.4–726.1	71.764 (1.254)	*Raskychara gobica*	632.3–807.1	72.861 (2.392)
Indeterminate interval	970–1456	81.385 (6.007)	*Ulmipollenites Ulmoideipites*	726.1–976.2	75.443 (3.679)	*Atopochara ulanensis*	807.1–1023.2	79.914 (7.053)
Strumosia inandita–Cypridea spangvosa	1456–1512	81.835 (0.45)	*Aquilapollenites*	976.2–1749	83.586 (8.143)			
Limnocypridea dilinensis Limnocypridea nova	1512–1607	82.566 (0.731)						
Periaca nthella portentosa Limnocypridea subscalariformis	1607–1734	83.474 (0.908)						
Cypridea liaukhenensis Cypridea bella	1734–1783.2	83.823 (0.349)						

input into lacustrine environments, resulting in higher Th values. We hypothesize that wetter and warmer climate conditions prevailed during the deposition of sediments when eccentricity was high.

(3) The C30n/C29r boundary is approximately one short eccentricity cycle above a 405-kyr eccentricity minimum in the Th record of K_2m^2 (Fig. 2), which is consistent with observations in marine strata (Husson et al., 2011; Westerhold et al., 2008; Batenburg et al., 2012).

4.3. Spectral analysis in the time domain

An important test of our astronomical interpretation is to conduct spectral analysis on the 405 kyr-tuned records. The power spectrum of the 405 kyr-tuned Th series of the K_2m and K_2s show significant spectral peaks with periodicities of eccentricity (2048 kyr, 405 kyr (tuned), 125 kyr, 120 kyr, 103 kyr and 90 kyr), obliquity (50 kyr, 45 kyr, 42.5 kyr and 38.4 kyr), and precession (23.2 kyr, 21.8 kyr, 19.6 kyr and 18.6 kyr) above the 99% confidence level (Fig. 7a). The power spectrum of the 405 kyr-tuned Th series of K_2n reveals peaks at eccentricity (405 kyr (tuned), 107 kyr and 90 kyr), obliquity (50.5 kyr and 38.3 kyr), and precession (22.3 kyr and 18.7 kyr) cycles above 95% confidence level (Fig. 7b). Wavelet analysis shows strong comparable spectral bands, and that the short eccentricity 'e' is modulated by long eccentricity 'E' (Fig. 7c and d). These spectral characteristics compare well with those of the La2010d and La2004 solutions and support our cyclostratigraphic interpretation (Fig. 3a, Laskar et al., 2004, 2011a).

5. Discussion

5.1. ATS of the SK-1n borehole

Cyclostratigraphic analysis of the untuned and 405 kyr-tuned Th series from the SK-1n borehole indicates that astronomical forcing strongly influenced the climate and environment of the SB during the Late Cretaceous. The new ATS of the SK-1n, which is tuned to the astronomical solution La2010d, provides a high-resolution time framework from Late Santonian to Early Danian (∼84 Ma–65 Ma) and can serve as a basis for precisely correlating the major geological, biological and geochemical events between Late Cretaceous marine and continental records (Fig. 6, Supplementary Table S2).

The astronomically calibrated formation and member boundary ages of the K_2m^2/K_2m^1, K_2m^1/K_2s, K_2n^5/K_2n^4, K_2n^4/K_2n^3, K_2n^3/K_2n^2 and K_2n^2/K_2n^1 are 70.496 Ma, 72.86 Ma, 80.695 Ma, 81.595 Ma, 82.392 Ma and 83.823 Ma, respectively. The ATS allows us to estimate the positions of the Cretaceous–Paleogene (K–Pg), Campanian–Maastrichtian, Santonian–Campanian boundaries at depths of 318 m, 752.8 m and 1751.1 m, considering an age of 66 Ma for the K/Pg boundary (Figs. 2–4, Supplementary Table S2).

The SK-1 borehole yields abundant microfossils. Detailed biozonations of spores/pollen, charophytes and ostracodes have been well defined (Xi et al., 2012; Wan et al., 2013; Qu et al., 2014). However, it is difficult to directly correlate these biozones to marine biota due to the absence of common fossils, which make them only have local correlation significance (Scott et al., 2012; Wan et al., 2013). The new ATS of the SK-1n can precisely estimate the ages and durations of the biozones, which provides high-resolution age constraints on the evolution of the lacustrine microfossils and allows us to correlate them to marine fossils (Fig. 6, Table 1). For example, the ostracode *Ilyocypris*, charophyte *G. changzhouensis–N. sinulata* and spore/pollen *Cedripites Piceapollis* zones represent the time of the latest Maastrichtian to earliest Danian (Fig. 6).

The SAR of the SK-1n borehole can be evaluated at the scale of 100 kyr eccentricity cycles that is constrained by 405 kyr eccentricity cycles (Figs. 2–4). The SAR of the K_2n increases from ∼14 cm/kyr in the lower part to ∼29.6 cm/kyr in the upper part, with an average of 19.2 cm/kyr. The SAR of the K_2m–K_2s varies between 3.2 and 12.5 cm/kyr with an average of 7.2 cm/kyr. High SAR of the upper K_2n is consistent with the basin margin uplift in response to accelerated subduction of the Pacific Plate (Feng et al., 2010).

5.2. *Position of the Cretaceous/Paleogene (K/Pg) boundary in the SK-1n borehole*

Despite the widespread occurrence of Cretaceous–Paleogene non-marine strata in China, the K/Pg boundary is rarely well-defined due to poor age constraint and a poor fossil record (Huang, 1988; Sha, 2007; Wan et al., 2007). The continuous stratigraphic records of the SK-1n borehole allow definition of the K/Pg boundary in the SB. Li et al. (2011) found a major palynofloral change at a depth of 360.6 m. However, pollen and spores are absent in the next 100-m-thick section (from 360.6 m to 263.4 m), implying that the K/Pg boundary could be above 360.6 m. Deng et al. (2013) proposed that the K/Pg boundary is somewhere in the depth interval of 317.03–342.1 m. Recently, Wan et al. (2013) estimated the boundary at 328 m after compiling the data of charophytes, palynology (Li et al., 2011) and magnetostratigraphy (Deng et al., 2013).

Cyclostratigraphic study of marine successions suggests that the position of the K/Pg boundary is located near the minimum of the first 405 kyr eccentricity cycle immediately above the base of chron C29r (Herbert, 1999; Kuiper et al., 2008; Westerhold et al., 2008; Hilgen et al., 2010; Husson et al., 2011; Batenburg et al., 2012), and that the duration between the K/Pg boundary and the base of the chron C29r is ∼300 kyr (Westerhold et al., 2008; Husson et al., 2011; Ogg, 2012). With this estimate and the depth of the C30n/C29r boundary at 342.1 m ± 1.4 m (Deng et al., 2013), our study indicates that the K/Pg boundary in the SK-1n borehole is at 318 m ± 1.2 m (Fig. 3), which is near the position estimated by Wan et al. (2013) but with a higher confidence.

5.3. *Duration of the hiatus between the Sifangtai (K_2s) and Nenjiang (K_2n) formations*

The regional unconformity marked by seismic horizon T03 separates the K_2s and K_2n, recording a regional uplift and weak structural inversion of the SB. This tectonic event led to abrupt change in depositional environments from deep lacustrine to fluvial and floodplain (Fig. 1, Feng et al., 2010). At the unconformity, clear stratal truncations are observed in the Northern Plunge zone and a slightly inclined angular unconformity is present in the eastern part of the SB. In the Central Depression Zone, up to 100 m strata of the Nenjiang Formation (K_2n^5) were eroded (Xin and Cai, 2004; Feng et al., 2010). However, there is no consistent estimate of the hiatus duration for this unconformity.

In this study, the ages of the lower boundary of the K_2s and upper boundary of the K_2n are identified as 76.077 Ma and 79.909 Ma (Fig. 6), respectively. Thus the duration of the hiatus is estimated as ∼3.8 myr, and the top of the chron C33r should be placed at the level of the unconformity (Deng et al., 2013). The time constraint for the hiatus at the unconformity improves the correlation between marine and continental records in the SB.

5.4. *Chron ages and durations*

The Late Cretaceous C-sequence (chrons C33r through C29r) has been studied in ocean-drilling cores and outcrops of pelagic sediments. Recently, Husson et al. (2011) and Thibault et al. (2012) estimated the ages and durations of each magnetochron from C32r.2r to C29n based on the Late Campanian–Maastrichtian 405-kyr eccentricity-tuned ATS from four ODP (Ocean Drilling Program) and DSDP (Deep Sea Drilling Program) holes. Ogg (2012) compiled the ages and durations of these chrons mainly from the

Table 2
Comparison between the published ages and durations of Upper Santonian–Lower Danian magnetic chron boundaries, and corresponding calculated sea floor spreading rate for the South Atlantic.

Chron	Distance (km) from South Atlantic Spreading Center (Cande and Kent, 1992)		This study (SK-IN core)				Option 2 of Husson et al. (2011)			CK95 (Cande and Kent, 1995)			GPTS2012 (Ogg, 2012)		
	Old End (km)	Width (km)	Depth (m)	Age (Ma)	Duration (myr)	Spreading rates (km/myr)	Age (Ma)	Duration (myr)	Spreading rates (km/myr)	Age (Ma)	Duration (myr)	Spreading rates (km/myr)	Age (Ma)	Duration (myr)	Spreading rates (km/myr)
C29r	1371.84	13.18	342.1 ± 1.4	66.30 ± 0.08			66.3 ± 0.08	0.300 ± 0.02		65.578	0.833		66.398	0.71	
C30n	1407.22	35.38					68.2 ± 0.08	1.9 ± 0.03	18.621	67.61	2.032	17.411	68.196	1.798	19.677
C30r	1409.56	2.34					68.32 ± 0.07	∼0.12	19.5	67.735	0.125	18.72	68.369	0.173	13.526
C31n	1429.14	19.58	530.78 ± 1.23	69.28 ± 0.09	2.98 ± 0.12 (C30n–C31n)	19.23	69.22 ± 0.07	∼0.9	21.756	68.737	1.002	19.541	69.269	0.9	21.756
C31r	1481.12	51.98	700.88 ± 0.38	71.46 ± 0.07	2.18 ± 0.11	23.844	71.4 ± 0.08	2.18 ± 0.03	23.844	71.071	2.334	22.271	71.449	2.18	23.844
C32n.1n	1487.68	6.56					71.64 ± 0.07	0.240 ± 0.06	27.333	71.338	0.267	24.569	71.689	0.24	27.333
C32n.1r	1493.94	6.26					71.72 ± 0.07	0.08 ± 0.03	78.25	71.587	0.249	25.141	71.939	0.25	25.040
C32n.2n	1531.81	37.87	852.6 ± 3.2	73.66 ± 0.12	2.20 ± 0.14 (C32n)	23.041	73.6 ± 0.08	1.88 ± 0.03	20.144	73.004	1.417	26.725	73.649	1.71	22.146
C32r.1r	1539.94	8.13	887.8 ± 0.7	74.24 ± 0.08	0.58 ± 0.14	14.017	73.9 ± 0.09	0.3 ± 0.06	27.100	73.291	0.287	28.328	73.949	0.3	27.100
C32r.1n	1542.32	2.38	895.8 ± 1.2	74.35 ± 0.09	0.11 ± 0.12	21.636	74 ± 0.08	0.1 ± 0.03	23.800	73.374	0.083	28.675	74.049	0.1	23.800
C32r.2r	1549.41	7.09	910.2 ± 0.6	74.55 ± 0.08	0.20 ± 0.12	35.45	74.1 ± 0.08	0.1 ± 0.04	70.900	73.619	0.245	28.939	74.309	0.26	27.269
C33n	1723.76	174.35	1020.4 ± 0.3							79.075	5.456	31.956	79.9	5.591	31.184
C33r	1862.32	138.56	1739.3 ± 0.4	83.51 ± 0.09	8.96 ± 0.12 (C33n–C33r)	34.923				83	3.925	35.302	83.64	3.74	37.048

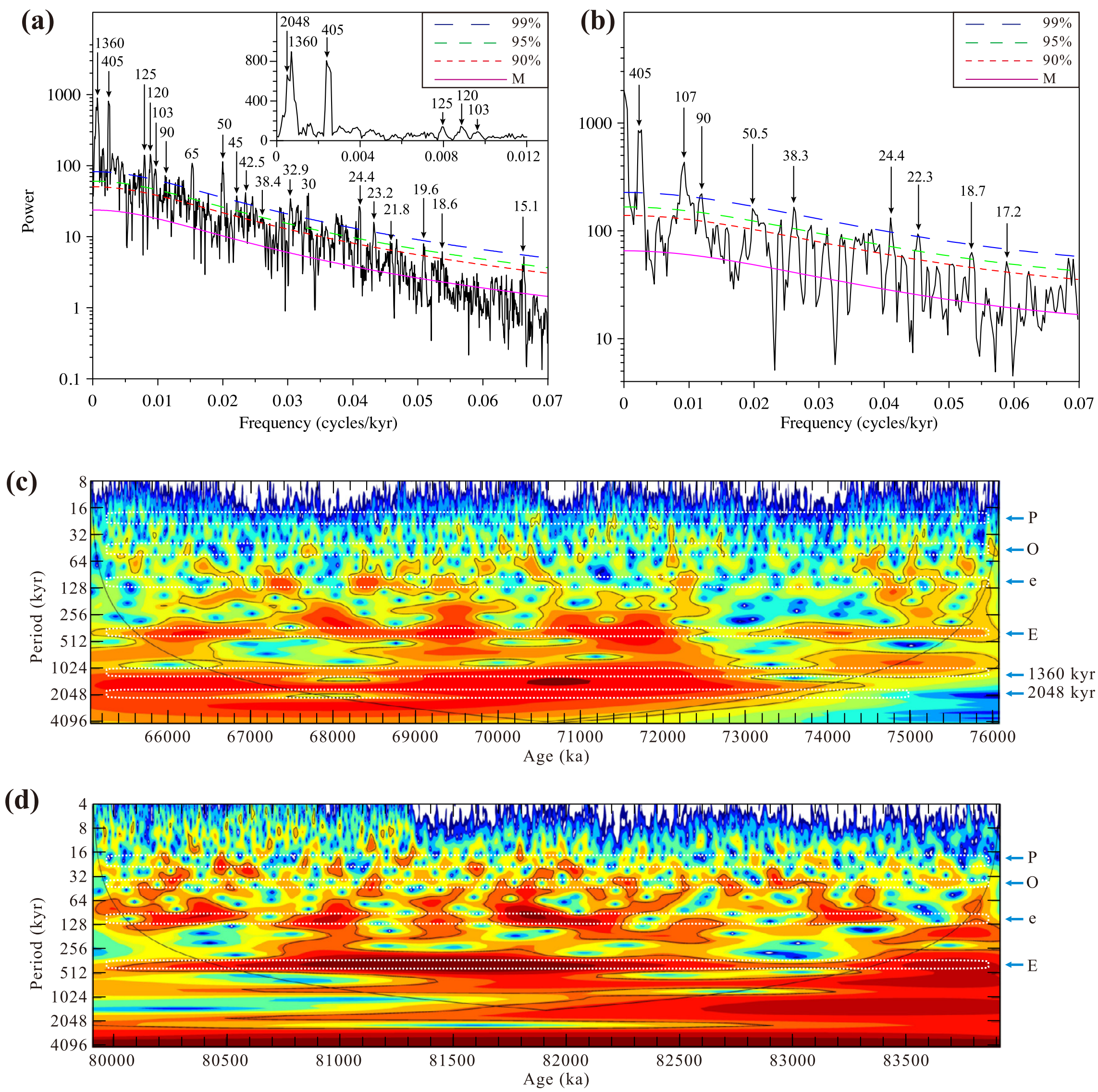

Fig. 7. 2π MTM power spectra (a, b) and Morlet wavelet scalograms (c, d) of the normalized 405-kyr tuned Th time series of the Mingshui (K_2m) and Sifangtai (K_2s) formations (a, c) and Nenjiang (K_2n) Formation (b, d) of the SK-1n borehole in the Songliao Basin. Frequency peaks are labeled in kyr. See legends and notes in Fig. 4. (For interpretation of the references to color in this figure legend, the reader is referred to the web version of this article.)

results of Husson et al. (2011) and Thibault et al. (2012) and applied the method of spline fit to marine magnetic anomaly widths.

Our ATS for the SK-1n core indicates that the ages of the base of chrons C29r, C31n, C31r and C32n.2n are 66.30 ± 0.08 Ma, 69.28 ± 0.09 Ma, 71.46 ± 0.07 Ma and 73.66 ± 0.07 Ma, and the durations between boundaries are 2.98 ± 0.12 myr (C30n–C31n), 2.18 ± 0.11 myr (C31r) and 2.2 ± 0.14 myr (C32n). These estimates are consistent with those of GPTS2012 (Ogg, 2012), Husson et al. (2011), Thibault et al. (2012) and Batenburg et al. (2012) within errors (Fig. 6a, Table 2). It also implies that our cyclostratigraphic interpretation and the ATS of SK-1n are reasonable and valid.

However, the lower ages (durations) of the chrons C32r.1r, C32r.1n and C32r.2r are calibrated as 74.24 ± 0.08 Ma (0.58 ± 0.14 myr), 74.35 ± 0.09 Ma (0.11 ± 0.12 myr) and 74.55 ± 0.08 Ma (0.20 ± 0.12 myr), which are older (and longer) than those in GTS2012 (Ogg, 2012) and the cyclostratigraphic estimate of Husson et al. (2011) (Fig. 6a, Table 2). Our results suggest a longer duration of 0.89 myr for the chron C32r, while Husson et al. (2011) and Ogg (2012) estimated 0.5 myr and 0.66 myr, respectively. Husson et al. (2011) estimated the durations for C32r.1r, C32r.1n and C32r.2r based on the cyclostratigraphy of the ODP Hole 762C. They interpreted that the upper part of C32r.1r was dominated by the 10–11 obliquity cycles, and this equals one 405-kyr eccentricity cycle, not their interpretation of two 100-kyr eccentricity cycles. Thibault et al. (2012) reinterpreted these same obliquity cycles as precession cycles, but this resulted in anomalous SAR and sea-floor spreading rates. Furthermore, the uncertainties of the chron boundaries in the ODP Hole 762C are very large. Our estimates of the ages and durations for C32r.1r–C32r.2r seem to be more reasonable and accurate because of the clear and well-defined 100-kyr and 405-kyr eccentricity cycles (Figs. 3, 5 and 6).

The boundary of C33r/C33n was placed at the depth 1020.4 m, 1.2 m above the major unconformity between the K_2s and K_2n, which results in a very low SAR for the lower K_2s (Deng et al., 2013). The polarity transition zone from C33r to C33n ranges from 1021.7 m to 1015.5 m (Deng et al., 2013). Combined with our results, the C33r/C33n boundary should be placed within the unconformity between K_2s and K_2n.

The C34n/C33r boundary in SK-1n is at the depth of 1739.3 ± 0.4 m (Deng et al., 2013), with an ATS age of 83.51 ± 0.09 Ma (Table 2), ∼100 kyr older than the estimated age of ∼83.4 Ma

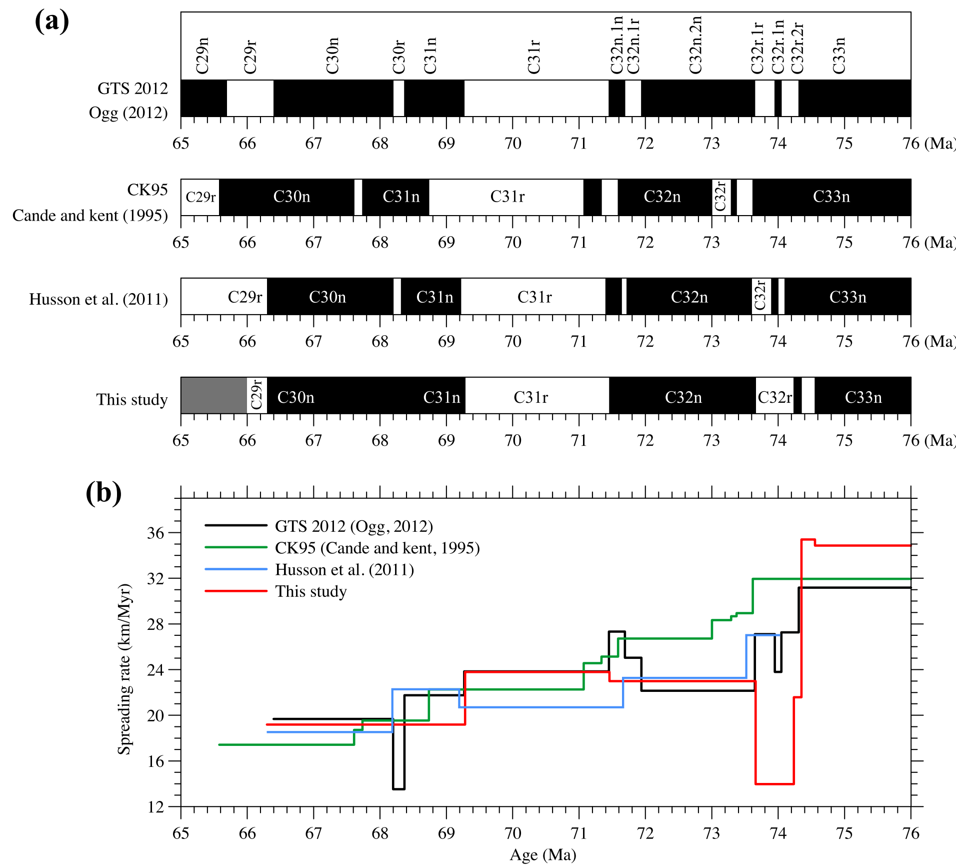

Fig. 8. (a) Comparison between the Late Cretaceous–Early Paleogene magnetostratigraphic time scales of GPTS2012 (Ogg, 2012), CK95 (Cande and Kent, 1995), Option 2 of Husson et al. (2011) and this study. (b) Comparison between calculated sea floor spreading rate of the South Atlantic through time based on the magnetostratigraphic time scales in (a).

(He et al., 2012), and ∼100 kyr younger than the tuning results in SK-1s (Wu et al., 2013c) and the estimate of Ogg (2012).

5.5. *Implications for the South Atlantic sea-floor spreading rates*

With the astronomically tuned ages and durations of polarity chrons in the SK-1n, we can assess variations of the Late Cretaceous portion (C33r–C29r) of the South Atlantic sea-floor spreading rates (Fig. 8b). From chrons C33r to C29r, spreading rates decreased from ∼35 km/myr to ∼18.6 km/myr on average. The general decline trend is consistent with the estimates of GTS2012 (Ogg, 2012), CK95 (Cande and Kent, 1995) and Husson et al. (2011) (Fig. 8b). However, the spreading rates of the magnetic anomalies of chrons C33r, C33n and C32r.2r is up to ∼35 km/myr, ∼3–4 km/myr higher than the results of CK95 (Cande and Kent, 1995) and GTS2012 (Ogg, 2012). Interestingly, we find an abrupt decrease of spreading rates down to 14 km/myr during chron C32r.1r, which might suggest large variations in spreading rates during the Late Cretaceous (see also Seton et al., 2009). If there was a consistent linear decrease of spreading rate between C33r and C30r, the low spreading rate at C32r.1r may reflect an underestimate for the width of this magnetic anomaly (8.4% 2σ error) (Table 2; Cande and Kent, 1992). Further study on the duration of C32r.1r and on the width of this magnetic anomaly in the South Atlantic sea-floor are needed to verify this apparent low spreading rate.

6. Conclusion

Cyclostratigraphic analysis of Late Santonian–Early Danian terrestrial strata of the SK-1n borehole reveals significant 405 kyr and 100 kyr eccentricity, obliquity and precession cycles, indicating astronomically controlled sedimentation in the terrestrial Songliao Basin of northeastern China. An astronomical time scale (ATS) for the sedimentary record of SK-1n is established by tuning the extracted 405-kyr cycles to La2010d astronomical solution based on the magnetostratigraphic time framework. The ATS provides high-resolution constraints on the ages and durations of the Late Cretaceous geological, biological and geophysical events:

(1) The 1541.6-m-long drillcore of the SK-1n covers about 18.85 myr from 83.92 Ma to 65.07 Ma (Late Santonian to Early Danian). The Cretaceous–Paleogene (K–Pg), Campanian–Maastrichtian, Santonian–Campanian boundaries are estimated at core depths of 318 m, 752.8 m and 1751.1 m, respectively.

(2) The lithological formation and member boundary ages of K_2m^2/K_2m^1, K_2m^1/K_2s, K_2n^5/K_2n^4, K_2n^4/K_2n^3, K_2n^3/K_2n^2 and K_2n^2/K_2n^1 are 70.496 Ma, 72.86 Ma, 80.695 Ma, 81.595 Ma, 82.392 Ma and 83.823 Ma, respectively.

(3) The duration of the late Santonian regional unconformity between K_2n and K_2s is ∼3.8 myr.

(4) The ages and durations of magnetochrons C33r to C30n are more confidently estimated than in previous attempts, and provide new numerical age constraints for the Late Cretaceous GPTS and South Atlantic sea-floor spreading rates.

Acknowledgements

We express our sincere appreciation to Prof. Chenglong Deng, Dr. Ross Nelson Mitchell and an anonymous reviewer for their useful comments that significantly improved the manuscript. This work was jointly supported by the National Key Basic Research Development Program of China (2012CB822002), the National Science

Foundation of China (41422202, 91128102) and Fundamental Research Funds for the Central Universities (2652012027).

Appendix A. Supplementary material

Supplementary material related to this article can be found online at http://dx.doi.org/10.1016/j.epsl.2014.09.038.

References

Batenburg, S.J., Sprovieri, M., Gale, A.S., Hilgen, F.J., Hüsing, S., Laskar, J., Liebrand, D., Lirer, F., Orue-Etxebarria, X., Pelosi, N., Smit, J., 2012. Cyclostratigraphy and astronomical tuning of the late Maastrichtian at Zumaia (Basque country, Spain). Earth Planet. Sci. Lett. 359–360, 264–278.

Cande, S.C., Kent, D.V., 1992. A new geomagnetic polarity time scale for the late Cretaceous and Cenozoic. J. Geophys. Res. 97, 13917–13951.

Cande, S.C., Kent, D.V., 1995. Revised calibration of the geomagnetic polarity timescale for the late Cretaceous and Cenozoic. J. Geophys. Res. 100, 6093–6095.

Chamberlain, C.P., Wan, X.Q., Graham, S.A., Carroll, A.R., Doebbert, A.C., Sageman, B.B., Blisniuk, P., Kent-Corson, M.L., Wang, Z., Wang, C.S., 2013. Stable isotopic evidence for climate and basin evolution of the Late Cretaceous Songliao basin, China. Palaeogeogr. Palaeoclimatol. Palaeoecol. 385, 106–124.

Chen, J.M., Zhao, P., Wang, C.S., Huang, Y.J., Cao, K., 2013. Modeling East Asian climate and impacts of atmospheric CO_2 concentration during the Late Cretaceous (66 Ma). Palaeogeogr. Palaeoclimatol. Palaeoecol. 385, 190–201.

Cheng, R.H., Wang, G.D., Wang, P.J., Gao, Y.F., Ren, Y.G., Wang, C.S., Wang, Q.Y., 2011. Centimeter-scale sedimentary sequence description of Upper Cretaceous–Lower Paleocene Mingshui Formation: lithostratigraphy, facies and cyclostratigraphy, based on the scientific drilling (SK1) borehole in the Songliao Basin. Earth Sci. Front. 18 (6), 285–328 (in Chinese with English abstract).

Cleveland, W.S., 1979. Robust locally weighted regression and smoothing scatterplots. J. Am. Stat. Assoc. 74, 829–836.

Deng, C.L., He, H.Y., Pan, Y.X., Zhu, R.X., 2013. Chronology of the terrestrial Upper Cretaceous in the Songliao Basin, northeast Asia. Palaeogeogr. Palaeoclimatol. Palaeoecol. 385, 44–54.

Feng, Z.Q., Jia, C.Z., Xie, X.N., Zhang, S., Feng, Z.H., Timothy, A.C., 2010. Tectonostratigraphic units and stratigraphic sequences of the nonmarine Songliao basin, northeast China. Basin Res. 22, 79–95.

Feng, Z.Q., Wang, C.S., Graham, S., Koeberl, C., Dong, H.L., Huang, Y.J., Gao, Y., 2013. Continental Scientific Drilling Project of Cretaceous Songliao Basin: scientific objectives and drilling technology. Palaeogeogr. Palaeoclimatol. Palaeoecol. 385, 6–16.

Gao, R.Q., Zhang, Y., Cui, T.C., 1994. Cretaceous Petroleum Bearing Strata in the Songliao Basin. Petroleum Industry Press, Beijing, pp. 1–333 (in Chinese with English abstract).

Gao, Y.F., Wang, P.J., Cheng, R.H., Wang, G.D., Wan, X.Q., Wu, H.Y., Wang, S.X., Liang, W.L., 2011. Centimeter-scale sedimentary sequence description of Upper Cretaceous Nenjiang Formation (lower members 1&2): lithostratigraphy, facies and cyclostratigraphy, based on the scientific drilling (SK1) borehole in the Songliao Basin. Earth Sci. Front. 18 (6), 195–217 (in Chinese with English abstract).

Gao, Y., Wang, C.S., Liu, Z.F., Zhao, B., Zhang, X.F., 2013. Clay mineralogy of the middle Mingshui Formation (upper Campanian to lower Maastrichtian) from the SKIn borehole in the Songliao Basin, NE China: implications for palaeoclimate and provenance. Palaeogeogr. Palaeoclimatol. Palaeoecol. 385, 162–170.

Ghil, M., Allen, M.R., Dettinger, M.D., Ide, K., Kondrashov, D., Mann, M.E., Robertson, A.W., Saunders, A., Tian, Y., Varadi, F., Yiou, P., 2002. Advanced spectral methods for climatic time series. Rev. Geophys. 40 (1), 3-1–3-41.

Gradstein, F.M., Ogg, J.G., Schmitz, M., Ogg, G. (Eds.), 2012. The Geologic Time Scale 2012. Elsevier, pp. 1–1127.

He, H.Y., Deng, C.L., Wang, P.J., Pan, Y.X., Zhu, R.X., 2012. Toward age determination of the termination of the Cretaceous Normal Superchron. Geochem. Geophys. Geosyst. 13, Q02002. http://dx.doi.org/10.1029/2011GC003901.

Herbert, T.D., 1999. Toward a composite orbital chronology for the late Cretaceous and early Paleocene GPTS. Philos. Trans. R. Soc. Lond. 357, 1891–1905.

Hilgen, F.J., Kuiper, K.F., Lourens, J.L., 2010. Evaluation of the astronomical time scale for the Paleocene and earliest Eocene. Earth Planet. Sci. Lett. 300, 139–151.

Hinnov, L.A., 2013. Cyclostratigraphy and its revolutionizing applications in the Earth and Planetary Sciences. GSA Bull. 125, 1703–1734.

Hinnov, L.A., Hilgen, F.J., 2012. Cyclostratigraphy and astrochronology. In: Gradstein, F.M., Ogg, J.G., Schmitz, M., Ogg, G. (Eds.), The Geologic Time Scale 2012. Elsevier, pp. 63–83.

Hinnov, L.A., Ogg, J.G., 2007. Cyclostratigraphy and the astronomical time scale. Stratigraphy 4, 239–251.

Huang, R., 1988. Charophytes of Nanxiong Basin, Guangdong and its Cretaceous–Tertiary Boundary. Acta Palaeontol. Sin. 27 (4), 457–474 (in Chinese with English abstract).

Huang, C.J., Hinnov, L., Fischer, A.G., Grippo, A., Herbert, T., 2010. Astronomical tuning of the Aptian Stage from Italian reference sections. Geology 38, 899–902.

Huang, Y.J., Yang, G.S., Gu, J., Wang, P.K., Huang, Q.H., Feng, Z.H., Feng, L.J., 2013. Marine incursion events in the Late Cretaceous Songliao Basin: constraints from sulfur geochemistry records. Palaeogeogr. Palaeoclimatol. Palaeoecol. 385, 152–161.

Husson, D., Galbrun, B., Laskar, J., Hinnov, L.A., Thibault, N., Gardin, S., Locklair, R.E., 2011. Astronomical calibration of the Maastrichtian (Late Cretaceous). Earth Planet. Sci. Lett. 305, 328–340.

Kodama, K.P., Hinnov, L.A., 2014. Rock Magnetic Cyclostratigraphy. Wiley–Blackwell Fast-Track Monograph. New Analytical Methods in Earth and Environmental Science Series, pp. 1–176.

Kuiper, K., Deino, A., Hilgen, F.J., Krijgsman, W., Renne, P.R., Wijbrans, J.R., 2008. Synchronizing rock clocks of Earth history. Science 320, 500–504.

Laskar, J., Robutel, P., Joutel, F., Gastineau, M., Correia, A.C.M., Levrard, B., 2004. A long term numerical solution for the insolation quantities of the Earth. Astron. Astrophys. 428, 261–285.

Laskar, J., Fienga, A., Gastineau, M., Manche, H., 2011a. La2010: a new orbital solution for the long-term motion of the Earth. Astron. Astrophys. 532, A89.

Laskar, J., Gastineau, M., Delisle, J.B., Farrés, A., Fienga, A., 2011b. Strong chaos induced by close encounters with Ceres and Vesta. Astron. Astrophys. 532, L4. http://dx.doi.org/10.1051/0004-6361/201117504.

Laurin, J., Čech, S., Uličný, D., Štaffen, Z., Svobodová, M., 2014. Astrochronology of the Late Turonian: implications for the behavior of the carbon cycle at the demise of peak greenhouse. Earth Planet. Sci. Lett. 394, 254–269.

Li, J.G., Batten, D.J., Zhang, Y.Y., 2011. Palynological record from a composite core through Late Cretaceous early Paleocene deposits in the Songliao Basin, Northeast China and its biostratigraphic implications. Cretac. Res. 32, 1–12.

Li, H.Y., Zhang, S.H., Wu, H.C., Zhao, K.L., Yang, T.S., Zhao, L., 2013. Rock magnetic records of the Qingshankou Formation of SK-1 south borehole in Songliao Basin, Northeast China, and their paleoclimate implications. Palaeogeogr. Palaeoclimatol. Palaeoecol. 385, 71–82.

Locklair, R.E., Sageman, B.B., 2008. Cyclostratigraphy of the Upper Cretaceous Niobrara Formation, Western Interior, U.S.A.: a Coniacian–Santonian orbital timescale. Earth Planet. Sci. Lett. 269, 540–553.

Mann, M.E., Lees, J.M., 1996. Robust estimation of background noise and signal detection in climatic time series. Clim. Change 33, 409–445.

Mayer, H., Appel, E., 1999. Milankovitch cyclicity and rock-magnetic signatures of palaeoclimatic change in the Early Cretaceous Biancone Formation of the Southern Alps, Italy. Cretac. Res. 20, 189–214.

Meyers, S.R., Siewert, S.E., Singer, B.S., Sageman, B.B., Condon, D.J., Obradovich, J.D., Jicha, B.R., Sawyer, D.A., 2012. Intercalibration of radioisotopic and astrochronologic time scales for the Cenomanian–Turonian boundary interval, Western Interior Basin, USA. Geology 40, 7–10.

Mitchell, R.N., Bice, D.M., Montanari, A., Cleaveland, L.C., Christianson, K.T., Coccioni, R., Hinnov, L.A., 2008. Ocean anoxic cycles? Prelude to the Livello Bonarelli (OAE 2). Earth Planet. Sci. Lett. 267, 1–16.

Ogg, J.G., 2012. Geomagnetic polarity time scale. In: Gradstein, F.M., Ogg, J.G., Schmitz, M., Ogg, G. (Eds.), The Geologic Time Scale 2012. Elsevier, pp. 85–113.

Okada, H., 2000. Nature and development of Cretaceous sedimentary basins in East Asia: a review. Geosci. J. 4, 271–282.

Paillard, D., Labeyrie, L., Yiou, P., 1996. Macintosh program performs time-series analysis. Eos 77, 379.

Pei, F.P., Xu, W.L., Yang, D.B., Zhao, Q.G., Liu, X.M., Hu, Z.C., 2007. Zircon U–Pb geochronology of basement metamorphic rocks in the Songliao Basin. Chin. Sci. Bull. 52, 942–948.

Qu, H.Y., Xi, D.P., Li, S., Colin, J.P., Huang, Q.H., Wan, X.Q., 2014. Late Cretaceous–early Paleocene ostracod biostratigraphy of scientific drilling SK1(n) in the Songliao Basin, northeast China. J. Paleontol. 88 (4), 786–789.

Ren, J.Y., Kensaku, T., Li, S.T., Zhang, J.X., 2002. Late Mesozoic and Cenozoic rifting and its dynamic setting in Eastern China and adjacent areas. Tectonophysics 344, 175–205.

Schnyder, J., Ruffell, A., Deconinck, J.-F., Baudin, F., 2006. Conjunctive use of spectral gamma-ray logs and clay mineralogy in defining late Jurassic–early Cretaceous palaeoclimate change (Dorset, UK). Palaeogeogr. Palaeoclimatol. Palaeoecol. 229, 303–320.

Scott, R.W., Wan, X.Q., Wang, C.S., Huang, Q.H., 2012. Late Cretaceous chronostratigraphy (Turonian–Maastrichtian): SK1 core Songliao Basin, China. Geosci. Front. 3 (4), 357–367.

Seton, M., Gaina, C., Müller, R.D., Heine, C., 2009. Mid-Cretaceous seafloor spreading pulse: fact or fiction? Geology 37 (8), 687–690.

Sha, J.G., 2007. Cretaceous stratigraphy of northeast China: non-marine and marine correlation. Cretac. Res. 28, 146–170.

Song, Z.G., Qin, Y., George, S.C., Wang, L., Guo, J.T., Feng, Z.H., 2013. A biomarker study of depositional paleoenvironments and source inputs for the massive formation of Upper Cretaceous lacustrine source rocks in the Songliao Basin, China. Palaeogeogr. Palaeoclimatol. Palaeoecol. 385, 137–151.

Sprovieri, M., Sabatino, N., Pelosi, N., Batenburg, S.J., Coccioni, C., Iavarone, M., Maxxola, S., 2013. Late Cretaceous orbitally-paced carbon isotope stratigraphy from the Bottaccione Gorge (Italy). Palaeogeogr. Palaeoclimatol. Palaeoecol. 379–380, 81–94.

Ten Veen, J.H., Postma, G., 1996. Astronomically forced variations in gamma-ray intensity: Late Miocene hemipelagic successions in the eastern Mediterranean basin as a test case. Geology 24, 15–18.

Thibault, N., Husson, D., Harlou, R., Gardin, S., Galbrun, B., Huret, E., Minoletti, F., 2012. Astronomical calibration of Upper Campanian–Maastrichtian carbon isotope events and calcareous plankton biostratigraphy in the Indian Ocean (ODP Hole 762C): implication for the age of the Campanian–Maastrichtian boundary. Palaeogeogr. Palaeoclimatol. Palaeoecol. 337–338, 52–71.

Torrence, C., Compo, G.P., 1998. A practical guide to wavelet analysis. Bull. Am. Meteorol. Soc. 79, 61–78.

Wan, X.Q., Chen, P.J., Wei, M.J., 2007. The Cretaceous system in China. Acta Geol. Sin. 81, 957–983.

Wan, X.Q., Zhao, J., Scott, R.W., Wang, P.J., Feng, Z.H., Huang, Q.H., Xi, D.P., 2013. Late Cretaceous Stratigraphy, Songliao Basin, NE China: SK1 cores. Palaeogeogr. Palaeoclimatol. Palaeoecol. 385, 31–43.

Wang, Y., Zhang, F.Q., Zhang, D.W., Miao, L.C., Li, T.S., Jie, W.Q., Meng, Q.R., Liu, D.Y., 2006. Zircon SHRIMP U–Pb dating of meta-diorite from the basement of the Songliao Basin and its geological significance. Chin. Sci. Bull. 51, 1877–1883.

Wang, P.J., Xie, X.A., Frank, M., Ren, Y.G., Zhu, D.F., Sun, X.M., 2007. The Cretaceous Songliao Basin: valcanogenic succession, sedimentary sequence and tectonic evolution, NE China. Acta Geol. Sin. 81, 1002–1011.

Wang, G.D., Cheng, R.H., Wang, P.J., Gao, Y.F., Wang, C.S., Ren, Y.G., Huang, Q.H., 2011a. Centimeter-scale sedimentary sequence description of Upper Cretaceous Sifangtai Formation: lithostratigraphy, facies and cyclostratigraphy, based on the scientific drilling (SK1) borehole in the Songliao Basin. Earth Sci. Front. 18 (6), 263–284 (in Chinese with English abstract).

Wang, P.J., Gao, Y.F., Cheng, R.H., Wang, G.D., Wu, H.Y., Wan, X.Q., Yang, G.S., Wang, Z.X., 2011b. Centimeter-scale sedimentary sequence description of Upper Cretaceous Nenjiang Formation (upper members 3–5): lithostratigraphy, facies and cyclostratigraphy, based on the scientific drilling (SK1) borehole in the Songliao Basin. Earth Sci. Front. 18 (6), 218–262 (in Chinese with English abstract).

Wang, C.S., Feng, Z.Q., Zhang, L.M., Huang, Y.J., Cao, K., Wang, P.J., Zhao, B., 2013a. Cretaceous paleogeography and paleoclimate and the setting of SKI borehole sites in Songliao Basin, northeast China. Palaeogeogr. Palaeoclimatol. Palaeoecol. 385, 17–30.

Wang, C.S., Scott, R.W., Wan, X.Q., Graham, S.A., Huang, Y.J., Wang, P.J., Wu, H.C., Dean, W.E., Zhang, L.M., 2013b. Late Cretaceous climate changes recorded in Eastern Asian lacustrine deposits and North American Epieric sea strata. Earth-Sci. Rev. 126, 275–299.

Weedon, G., 2003. Time-Series Analysis and Cyclostratigraphy. Cambridge University Press, Cambridge, pp. 1–259.

Westerhold, T., Röhl, U., Raffi, I., Fornaciari, E., Monechi, S., Reale, V., Bowles, J., Evans, H.F., 2008. Astronomical calibration of the Paleocene time. Palaeogeogr. Palaeoclimatol. Palaeoecol. 257 (4), 377–403.

Westerhold, T., Röhl, U., Laskar, J., 2012. Time scale controversy: accurate orbital calibration of the early Paleogene. Geochem. Geophys. Geosyst. 13, Q06015. http://dx.doi.org/10.1029/2012gc004096.

Wu, H.C., Zhang, S.H., Jiang, G.Q., Huang, Q.H., 2009. The floating astronomical time scale for the terrestrial Late Cretaceous Qingshankou Formation from the Songliao Basin of Northeast China and its stratigraphic and paleoclimate implications. Earth Planet. Sci. Lett. 278, 308–323.

Wu, H.C., Zhang, S.H., Feng, Q.L., Jiang, G.Q., Li, H.Y., Yang, T.S., 2012. Milankovitch and sub-Milankovitch cycles of the Early Triassic Daye Formation, South China and their geochronological and paleoclimatic implications. Gondwana Res. 22 (2), 748–759.

Wu, H.C., Zhang, S.H., Hinnov, L., Feng, Q.L., Jiang, G.Q., Li, H.Y., Yang, T.S., 2013a. Time-calibrated Milankovitch cycles for the late Permian. Nat. Commun. 4, 2452. http://dx.doi.org/10.1038/ncomms3452.

Wu, H.C., Zhang, S.H., Jiang, G.Q., Hinnov, L., Yang, T.S., Li, H.Y., Wan, X.Q., Wang, C.S., 2013c. Astrochronology of the Early Turonian–Early Campanian terrestrial succession in Songliao Basin, northeastern China and its implication for the long-period behavior of the Solar System. Palaeogeogr. Palaeoclimatol. Palaeoecol. 385, 55–70.

Wu, H.C., Zhang, S.H., Jiang, G.Q., Yang, T.S., Guo, J.H., Li, H.Y., 2013b. Astrochronology for the Early Cretaceous Jehol Biota in Northeastern China. Palaeogeogr. Palaeoclimatol. Palaeoecol. 385, 221–228.

Xi, D.P., Li, S., Wan, X.Q., Jing, X., Huang, Q.H., Colin, J.P., Wang, Z., Si, W.M., 2012. Late Cretaceous biostratigraphy and paleoenvironmental reconstruction based on non-marine ostracodes from well SK1 (south), Songliao Basin, northeast China. Hydrobiologia 688, 113–123.

Xin, R.C., Cai, X.Y., 2004. Controls of buried history on oil accumulation processes in Daqing placanticline of Northern Songliao Basion. Earth Sci., J. China Univ. Geosci. 29 (4), 457–460 (in Chinese with English abstract).